MODELING HEATSHIELD EROSION DUE TO DUST PARTICLE IMPACTS FOR A MARTIAN ENTRY VEHICLE

G. Palmer[1], E. Ching[2], M. Ihme[2], D. Kerkhoff[3], and A. Gülhan[3]

[1]AMA, Inc., Mail Stop 230-2, NASA Ames Research Center, Moffett Field, CA 94035, grant.e.palmer@nasa.gov, [2]Department of Mechanical Engineering, Stanford University, Stanford, CA 94305, eching@stanford.edu, mihme@stanford.edu, [3]Institute of Aerodynamics and Flow Technology, DLR, ali.guelhan@dlr.de, dirk.kerkhoff@dlr.de

ABSTRACT

The modeling assumptions and governing equations required to estimate the heatshield surface recession due to dust particle impacts are presented. The dust particle size distribution can be estimated using a modified gamma distribution. The vertical distribution of dust particles in the atmosphere in terms of the ratio of dust particle to atmospheric density can be related to measured or computed values of the dust opacity. The different approaches to coupling the particle and fluid dynamics are discussed. The equations and modeling assumptions presented in this paper are applied to computing the surface recession due to dust particle impacts on the ExoMars Schiaparelli capsule entering the Martian atmosphere during a representative dust storm. The dust surface recession at the stagnation point of about 1 mm is about 40% of the recession value due to charring ablation.

1. NOMENCLATURE

C_D = drag coefficient
c_p = specific heat of dust particle, J/kg-K
d_p = dust particle diameter, m
D_c = impact crater diameter, m
$d_z\tau$ = dust opacity, 1/km
h = heat transfer coefficient, W/m^2-K
$N(r)$ = particle distribution
N_v = volumetric number density, 1/m^3
p = pressure, N/m^2, or penetration depth, m
q = mass mixing ratio, ρ_{dust}/ρ
r_{eff} = effective particle radius, m
r_m = mode radius, m
r_p = dust particle radius, m
T = fluid temperature, K
T_p = particle surface temperature, K
ρ = atmospheric density, kg/m^3
ρ_d = dust particle density, kg/m^3
τ = optical depth
v_p = dust particle impact velocity, m/s

2. INTRODUCTION

One of the unique aspects of designing a spacecraft that will enter the Martian atmosphere is the need to account for the presence of dust. Small dust particles are present even under quiescent conditions, and the level of dust significantly increases when a major dust storm occurs. During or after a dust storm, the dust can extend to altitudes as high as 50 km [1].

Based on observations taken over decades, major global dust storms occur on the average of once every 3–4 Earth years. They do not, however, happen at regular intervals. For example, two major global dust storms occurred in 1977. Based on measurements taken by the Viking landers and estimations of the strength of the vertical winds in the Martian atmosphere, it was determined that the residence time of the larger (5–10 μm diameter) particles in the upper atmosphere was between 20 and 50 days after the beginning of a major dust storm [1].

Because planetary missions to Mars take years from initial design to arrival at Mars, and because of the unpredictability of major global dust storms, the design of the thermal protection system (TPS) of a Mars entry vehicle requires an estimation for the potential damage caused by dust particle impacts on the heatshield. This paper will provide an overview of the equations and modeling assumptions that go into an analysis of heatshield erosion due to dust particle impacts during a Martian entry and will apply these techniques to estimate the heatshield erosion on the ExoMars Schiaparelli capsule.

3. PARTICLE SIZE DISTRIBUTION

Toon, et al. [2] deduced from the Mariner 9 data that the dust particle shapes were plate-like, but most researchers (e.g. Refs. [2] – [4]) assume that the particles are spherical, and this assumption was used in the present study. In addition, the dust particles were assumed to be of uniform composition. Estimates of dust particle density in the literature range from 2400 – 3000 kg/m^3. Papadopoulos, et al. [3] assumed a particle composition of 70% SiO_2, 15-20% Al_2O_3, with the rest being iron oxides and trace compounds. The value of dust

particle density recommended in Ref. [3] of 2940 kg/m^3 was used in this study.

Based on analysis of the Mariner 9 spectrometer data taken during the 1971 dust storm, a Martian dust particle size distribution was derived based on a modified gamma distribution [2].

$$N(r) = cr_p^2 exp\left(-4\left({}^{r_p}/_{r_m}\right)^{0.5}\right) \quad (1)$$

The value of the constant, c, in Eq. (1) is arbitrary, because its value cancels out when the gamma distribution is normalized. Decreasing the value of the mode radius, r_m, shifts the gamma distribution curve to the left increasing the number of smaller-radius particles. Earlier studies such as Toon, et al. [2] and Refs. [3] and [4] used a value of 0.4e-6 m for the mode radius. However, more recent observations by the Mars Climate Sounder (MCS) [5] and computations using the NASA Ames General Circulation Model (GCM) [6] indicate that a smaller mode radius value is a better match to that data. A value of 3.5 micron was used in this study. The modified gamma distribution used in this study is shown in Fig. 1.

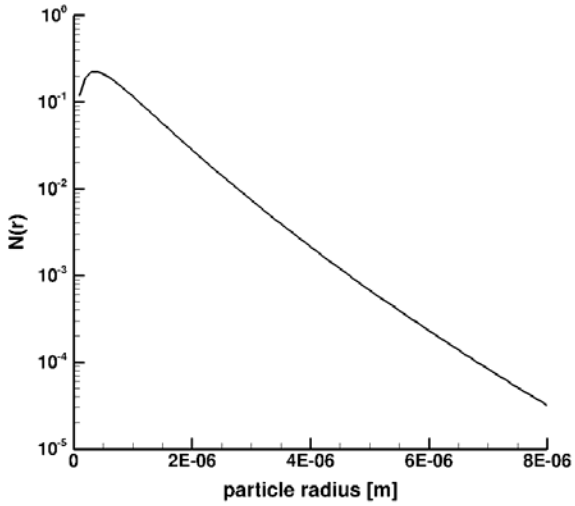

Figure 1. Modified gamma distribution.

To obtain the fractional amount of each particle radius in the distribution (i.e. the number fraction), the gamma distribution value for that radius is divided by the integral of the gamma distribution over all particle radii considered. Assuming that the composition of particles of different radii is the same, the mass fraction of a given particle radius, a value required for the damage assessment, is found by multiplying the gamma distribution for a given radius by the spherical volume for that radius divided by the integral of those two quantities over the entire distribution.

The number and mass fractions for the modified gamma distribution with a mode radius of 3.5 micron is shown in Fig. 2. In terms of number fraction, the most prevalent particle radius is 0.4 micron. The mass fractions are more weighted to the larger radius values, and the radius with the largest mass fraction is 2.2 micron.

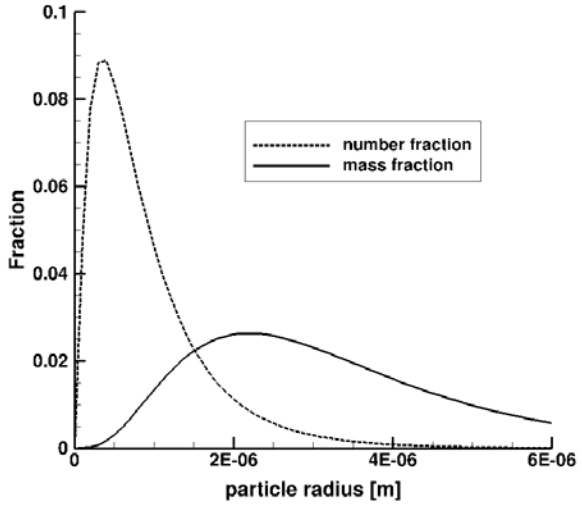

Figure 2. Number and mass fractions as a function of particle radius.

Since it is impractical to consider every possible particle radius in a particle damage assessment, in this study 15 particle radii values were considered. The mass fractions over the entire distribution were binned together into the 15 discrete particle radii values ranging from 0.5 to 9 microns shown in Fig. 3. The 2.0 and 2.5 micron radius particles have the largest mass fractions in the binned distribution.

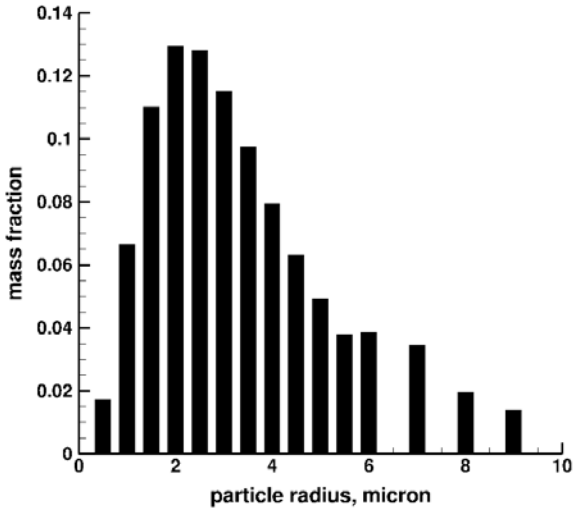

Figure 3. Particle mass fractions.

4. VERTICAL DISTRIBUTION OF DUST IN THE MARTIAN ATMOSPHERE

The MCS system on Mars Reconnaissance Orbiter (MRO) has been making global, moderate vertical resolution observations of infrared radiance in nine broadband channels sensitive to dust, temperature, and other aerosols. Atmospheric retrievals from MCS observations include vertical profiles of temperature and dust opacity, i.e., fractional extinction due to dust per unit height, $d_z\tau$, [5]. The MCS retrieval algorithm was based on the dust being compositionally uniform and made of spherically symmetric particles with a modified gamma size distribution of the form shown in Eq. (1).

The opacity can be related to the volumetric number density (i.e. the number of dust particles per unit volume), N_v.

$$d_z\tau = N_v Q_{ext} \int_0^\infty \pi r^2 N(r) dr = N_v Q_{ext} G \quad (2)$$

The quantity, Q_{ext}, is a dimensionless constant. The MCS retrieval algorithm set its value to be 0.35 [5]. The quantity in the integral, G, is the average geometric cross section of the particle distribution assuming a circular cross section shape.

The mass mixing ratio, q, is the ratio of the mass of dust in the atmosphere per unit volume divided by the mass of atmospheric gas per unit volume. Toon, et al. [2] define the mass of dust per unit volume using the average (spherical) particle volume of the distribution.

$$q = \frac{\rho_d N_v}{\rho} \int_0^\infty \frac{4}{3} \pi r^3 N(r) dr \quad (3)$$

To simplify Eq. (3), the effective particle radius, r_{eff}, is defined as the following.

$$r_{eff} = \frac{\int_0^\infty r^3 N(r) dr}{\int_0^\infty r^2 N(r) dr} \quad (4)$$

The effective radius is a function of the mode radius. Decreasing the mode radius shifts the distribution function to the left (i.e. to smaller particle radii) and reduces the effective radius. Using the effective radius, the mass mixing ratio equation can be expressed in terms of the density ratio of the dust and atmosphere, the opacity, and the effective radius.

$$q = \frac{4}{3} \frac{\rho_d}{Q_{ext}} \frac{d_z\tau}{\rho} r_{eff} \quad (5)$$

The quantity, $\frac{d_z\tau}{\rho}$, is known as the density-scaled opacity and has units of m^2/kg, which implies that the units of the opacity must be converted from km^{-1} to m^{-1} before dividing by the atmospheric density. Based on Eq. (5), if the density-scaled opacity is increased, the mass mixing ratio will increase by a proportional amount.

It was desired in this study to model a severe dust storm, so a density-scaled opacity value of 1.1e-3 m^2/kg was specified at an altitude of 20 km. This value, while high, is within the bounds of the MCS data shown in Ref. [5]. The modified gamma distribution with a mode radius of 3.5 microns yields an effective radius of 2.38 microns, which is inside the range of values from Ref. [6]. Assuming a value for Q_{ext} of 0.35 results in a mass mixing value of 2.940e-5 at 20 km altitude. This value is similar to that shown at a 20 km altitude in Ref. [4].

Due to the effects of sedimentation and mixing during a global dust storm, Conrath [7] derived an equation to account for the mass mixing ratio decreasing with increasing altitude. Originally expressed in terms of a scale height, it is common (e.g. Refs. [5] and [6]) to define the mass mixing ratio at a given altitude as a function of the mass mixing ratio at the surface, q_0 , and the ratio of the pressure at the desired altitude to the surface pressure, p_0, which is approximately 700 N/m^2.

$$q = q_0 exp\left[\upsilon\left(1 - {}^{p_0}/_{p}\right)\right] \quad (6)$$

The quantity, υ, is known as the Conrath parameter and represents the ratio between the characteristic dust diffusion time and characteristic dust sedimentation time at the surface. Kahre, et al. [4] suggested that a Conrath parameter of 0.05 was the best fit to their simulation using the NASA Ames General Circulation Model. However, Forget, et al. [8] recommended a value of 0.007 as a fit to the Mariner 9 data of the 1971 dust storm. Decreasing the value of the Conrath parameter increases the mass mixing ratio at higher altitudes. In this study, a Conrath parameter value of 0.01 was used to represent one of the more severe dust conditions shown in Ref. [5] where significant dust levels exist at altitudes as high as 45 km.

5. PARTICLE IMPACT DAMAGE MODELS

When a dust particle strikes the surface of the heatshield with sufficient energy, the resulting impact crater and material loss will increase the rate of surface erosion. The surface damage models used by Papadopoulos, et al. [3] and Palmer, et al. [4] were based on Apollo-era experiments where 0.4 – 1.58 mm diameter spheres made from pyrex, aluminum, and sapphire were fired at fused silica targets to develop damage models for micro-meteor impacts on the windows of the Mercury, Gemini, and Apollo spacecraft [9]. The velocity range of the particles was between 0.17 – 7.48 km/s.

Papadopoulos, et al. [3] developed a model for simulating heatshield erosion due to dust particle impact in the Martian atmosphere that was based on the data from Ref. [9]. Because the Martian dust particle composition is largely silicate-based, the pyrex projectile data from Ref. [9] was deemed to be the most appropriate available empirical data to use in the Martian damage model. Based on this data, correlations were developed for crater diameter, D_c, and penetration depth, p,

for glassy and AVCOAT heatshields as a function of particle diameter and velocity at impact.

Glassy TPS:

$$\frac{D_c}{d_p} = 0.113 v_p^{0.667} \qquad \frac{p}{d_p} = 0.3016 d_p^{0.4} v_p^{0.667} \qquad (7)$$

AVCOAT:

$$\frac{p}{d_p} = 0.024 v_p^{0.667} \qquad \frac{D_c}{d_p} = 0.048 v_p^{0.667} \qquad (8)$$

In Ref. [3], the relations for glassy TPS were assumed to be applicable to materials such as Shuttle tiles. The damage correlation for AVCOAT shown in Eq. (8) takes into account that the surface may be charred due to ablation. The AVCOAT crater was assumed to be hemispherical (the glass crater was not), which is why the AVCOAT crater diameter is simply twice the penetration depth. One interesting thing to note about Eqs. (7) and (8) is that the penetration depth and crater diameter are not functions of the particle density (i.e. mass) but only depend on the particle diameter and velocity at impact, but this may be due to the assumption of spherical particles of uniform composition where particle mass can be expressed in terms of particle diameter.

Another set of data was taken at the NASA JSC Hypervelocity Impact Research Laboratory [10] where aluminum spheres and nylon cylinders were fired at LI-900 and LI-2200 Shuttle tiles at velocities up to 7.1 km/s in order to develop impact damage models for those materials. The resulting correlations are functions of the density ratio between the projectile and material and account for the impact angle, θ.

$$\frac{p}{d_p} = 1.27 \left(\frac{\rho_p}{\rho_t}\right)^{0.5} \left(v_p \cos\theta\right)^{0.667} \qquad (9)$$

$$\frac{D_c}{d_p} = 1.85 {\rho_p}^{0.333} (1 + 0.25 \sin\theta)^{0.667} \left(v_p\right)^{0.667} \qquad (10)$$

The damage model from Ref. [10] does not assume hemispherical craters, so the D_c parameter in Eq. (10) represents the maximum crater diameter. The units for the crater diameter and penetration depth in Eqs. (9) and (10) are mm, the density is gm/cm^3, and the particle velocity is km/s.

The experimental data from Refs. [9] and [10] were based on projectiles that were two orders of magnitude larger than what will be experienced in the Martian atmosphere. In order to obtain data with more relevant particle sizes, a series of experiments are planned in the DLR GBK experimental facility that will include the capability to inject particles into the wind tunnel flow. Once that data is available, updated surface damage correlations will be developed for more representative particle diameters, and results from the updated models will be compared with results using the legacy damage models.

6. PARTICLE TRAJECTORY ANALYSIS

The particle surface damage models used in this paper relate the size of the crater caused by particle impact to the diameter and velocity of the particle when it strikes the heatshield. As a spacecraft enters the Martian atmosphere, any dust particles suspended in the atmosphere will strike the bow shock wave in front of the heatshield. As the dust particles travel through the shock layer towards the heatshield, the fluid will slow down and heat the surface of the particles. Depending on the size of the particles and the freestream velocity and altitude, the particles may be carried around the heatshield and not strike it at all.

There are different ways of modeling the particle trajectory through the shock layer depending on the degree of fidelity that is desired. The approach used by Refs. [3] and [4] was to assume that the particles are small enough and disperse enough that they do not affect the fluid in the shock layer and do not collide with each other. This approach is referred to as one-way coupling. The flow solution can be computed first using a CFD code. The particle trajectories are then computed using the underlying flow solution.

The particle trajectory analysis for the one-way coupling approach uses a Lagrangian method where the location, velocity, diameter, and temperature of an individual particle is updated as it travels through the shock layer by solving a series of coupled ordinary differential equations (ODEs).

Dust particles traveling through the shock layer follow the streamlines of the surrounding fluid, but the velocity of the dust particles will be different from the flow velocity in that dust particle velocity will typically be higher. The time rate of change of dust particle velocity magnitude is modeled by equating Newton's second law of motion with the equation for aerodynamic drag for a spherical particle of uniform composition.

$$\frac{d\overrightarrow{V_p}}{dt} = \frac{3}{4} \frac{\rho}{\rho_p} \frac{C_D}{d_p} (\Delta V^2) \qquad (11)$$

The velocity term on the right-hand side of Eq. (11), ΔV, is the relative velocity between the dust particle and the surrounding fluid. Equation (11) represents the magnitude of the change in velocity in that its value will always be positive. The particles will generally slow down as they travel through the shock layer (a positive $d\overrightarrow{V_p}$ value would imply they were speeding up), so the result from Eq. (11) must be multiplied by the signed values of the relative velocity components.

Martian dust particles are small enough that they will predominantly be in the transitional or free molecular flow regimes as they travel through the shock layer. Typical Knudsen numbers based on particle diameter will be greater than 0.1 at lower altitudes and can exceed 2 at altitudes greater than 50 km. In this study, the drag coefficient is computed using the Henderson model [11], which is applicable for continuum, transitional, and free-molecular

flow regimes. The Henderson correlation estimates drag coefficient as a function of the particle Mach and Reynolds number, values evaluated using the particle diameter and the relative particle velocity. Generally speaking, the particle Mach numbers in the shock layer will be supersonic, and the particle Reynolds numbers will be on the order of 1.

As the dust particle travels through the shock layer, energy is transferred to it from the surrounding fluid, and the surface temperature of the dust particle will increase. The particles are assumed to be small enough that there is no temperature gradient through the particle. Neglecting radiative heating, the rate of change of particle energy per unit volume is equal to the convective heat transfer over the entire surface of the particle divided by the particle volume. Because the particles are assumed to be spherical, the change in particle surface temperature can be expressed in terms of the convective heating rate and dust particle diameter.

$$\frac{dT_p}{dt} = \frac{6h}{\rho_p c_p d_p}\left(T - T_p\right) \tag{12}$$

The heat transfer coefficient, h, in Eq. (12) can be related to the Nusselt number, Nu, which represents the ratio of convective to conductive heat transfer across a boundary. In this study, the Nusselt number correlation developed by Fox, et al. [12] is used that accounts for non-continuum effects and is valid for subsonic and supersonic particle Mach numbers.

As the particles travel through the shock layer, heat is transferred to the surface of the particles from the surrounding fluid. If the surface temperature of the particles exceeds the vaporization temperature, vaporization will occur causing the dust particles to shrink. The one-way coupling method presented in this paper assumes that once the vaporization temperature is reached, any additional energy transfer to the surface of the particle is assumed to go into material vaporization. For spherical particles, the rate of change of particle diameter due to vaporization is a function of the vaporization temperature, T_{vap}, and the latent heat of vaporization, ζ.

$$\frac{d(d_p)}{dt} = \frac{2h(T - T_{vap})}{\zeta \rho_p} \tag{13}$$

The final ODEs in the coupled set of equations update the location of the particle in the shock layer. For 2-D particle tracing analysis, there would be two additional ODEs.

$$\frac{dx_p}{dt} = u_p \tag{14}$$

$$\frac{dy_p}{dt} = v_p \tag{15}$$

In this study, the set of particle tracing ODE's was solved using a 4th-order Runge-Kutta technique. Starting from a location along the outer boundary of the CFD grid, the particle trajectories were updated using a suitably-small time step until either the particles strike the surface of the heatshield or disappear due to vaporization.

The next level of fluid-particle analysis fidelity is known as two-way coupling where the particles and shock layer fluid can exchange momentum and energy. An example of this approach is the work of Ching, et al. [13] where a Lagrangian particle method is incorporated into a discontinuous Galerkin (DG) framework. Two-way coupling codes can model phenomena such as thermophoretic heating due to a temperature difference between the windward and leeward surfaces of a particle that one-way codes cannot. Also, it has been shown experimentally that the presence of particles can augment surface heating due to energy transfer in the boundary layer and wall collision, another effect that one-way coupling codes are unable to model.

7. THE ICARUS MATERIAL RESPONSE SOLVER

The Icarus material response solver is a three-dimensional, unstructured code developed at NASA Ames that solves the finite-volume formulation of the material response equations including the effects of material decomposition and ablation [14]. A surface erosion boundary condition has been implemented in Icarus that solves a surface energy balance that includes the effects of charring ablator mass flow, pyrolysis gas flow, and surface ablation due to particle impacts. The surface damage correlations for glassy TPS and AVOCAT, shown in Eqs. (7) and (8) have been incorporated into the Icarus erosion boundary condition. The surface erosion inputs into Icarus are the particle diameter, velocity, and number of particles per unit area striking the heatshield. These inputs can be both time- and spatially-varying.

8. DUST EROSION ON THE EXOMARS SCHIAPARELLI CAPSULE

In order to demonstrate the one-way coupling approach, it was applied to compute the theoretical dust erosion on the ExoMars Schiaparelli capsule [15] during its October 2016 descent into the Martian atmosphere. The Schiaparelli entry capsule included a heatshield that was a 2.4 m diameter, 70 deg sphere cone. One of the mission goals of Schiaparelli was to enter the Martian atmosphere during a time of year when dust storms are more likely to occur in order to (hopefully) perform atmospheric and surface measurements in the dust-rich environment. Unfortunately, a dust storm did not occur when Schiaparelli began its descent, but detailed trajectory information on the Schiaparelli entry is available to perform a dust erosion analysis.

In order to provide the flow solutions necessary for the particle trajectory analysis, 3-D CFD solutions were generated at 10 trajectory points using the DPLR Navier-Stokes flow solver [16]. For the Schiaparelli solutions, an 8-species [CO_2, CO, N_2, O_2, NO, C, N, O] finite-rate chemistry model was used. Thermochemical non-equilibrium was simulated using a two-temperature (T-Tv) model. A fully-

catalytic, radiative equilibrium wall boundary condition was used. The CFD trajectory points are shown in Fig. 4. The five lowest altitude points are known in the literature [15] as Schiaparelli trajectory points S2 through S5. In addition to these trajectory points, five additional, higher-altitude points were selected at 5 km intervals up to an altitude of 50 km.

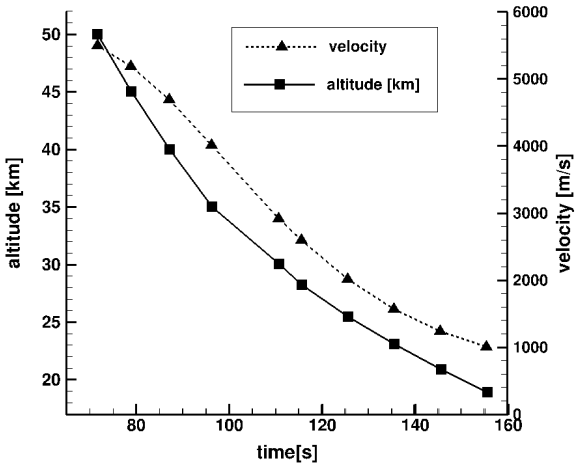

Figure 4. CFD trajectory points

The Schiaparelli entry trajectory is relatively benign in terms of heating rate with a peak stagnation point convective heating rate of about 45 W/cm^2 at the 45 km trajectory point. Once the CFD solutions were complete for the 10 trajectory points, flow data (density, velocity, temperature, thermal conductivity, etc.) was extracted on the symmetry plane to provide the underlying shock layer fluid data required by the 2-D particle trajectory code.

The particle trajectory code was then run at each of the trajectory points for each of the 15 particle diameter values listed in Fig. 3. In order to get a distribution of particle diameters and velocities along the surface, particle trajectories were computed at 101 evenly-spaced starting locations along the outer boundary of the CFD grid. The particle trajectory code then updated the particle location and state by solving the set of coupled ODEs described in Section 6 until the particle either struck the surface or was deflected around the heatshield. In certain situations where the freestream velocity was low, the particle would slow down enough so it would be "captured" by the boundary layer and never reach the surface. In this case the particle trajectory simulation was halted after a sufficiently long simulation time.

Smaller particles are slowed down and deflected more by the surrounding flow than are larger particles, and the surface temperature of the smaller particles reaches higher levels due to the increased surface heating rate for smaller particles. An example of the trajectories of small particles is shown in Fig. 5 where six 1-micron diameter particles starting at different locations along the outer boundary of the CFD grid travel through the shock layer at 30 km altitude. The circles represent particle location, and the color inside the circle denotes the particle velocity. In this situation, most of the 1-micron particle are deflected enough by the flow that they miss the heatshield. In contrast, when 5-micron diameter particles are simulated, the deceleration and deflection is greatly reduced, and every particle except the one started at the y = -1.25 location strikes the heatshield.

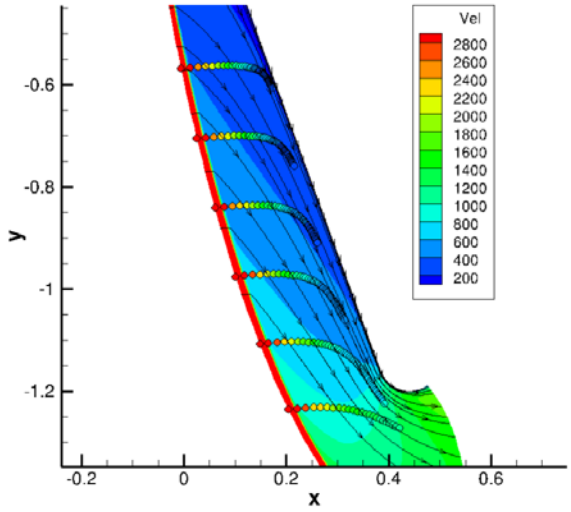

Figure 5. Trajectories of 1-micron diameter particles through the shock layer, 30 km altitude

For the Schiaparelli simulation, the 1-micron diameter particles experience the highest surface temperature increase. The peak temperature is slightly less than the vaporization temperature. Changes to the entry trajectory (i.e. making it steeper) or to assumptions that go into the heat transfer coefficient or material properties might cause the smaller particles to exceed the vaporization temperature, but for the results presented in this paper all of the particles maintained their original size.

The particle impact velocity on the heatshield is a function of particle size and the initial particle location in the shock layer. Figure 6 show impact velocities as a function of particle size at the 35 km trajectory point. The freestream velocity at this trajectory point is 4017 m/s. The x-axis represents vertical location along the symmetry plane of the capsule with the center of the heatshield at y=0. Along the stagnation line, close to y=0, the shock layer is thinnest, so the particles pass through the shock layer relatively quickly with less time to decelerate into the fluid. As the initial particle location moves away from the stagnation line, the shock layer is thicker, so the particles slow down to a greater extent. The amount of deceleration is a function of the particle size. Particles with diameters equal to or greater than 9 microns experience very little deceleration and strike the heatshield at nearly the freestream velocity. The asymmetry in Fig. 6 is due to the slight angle of attack.

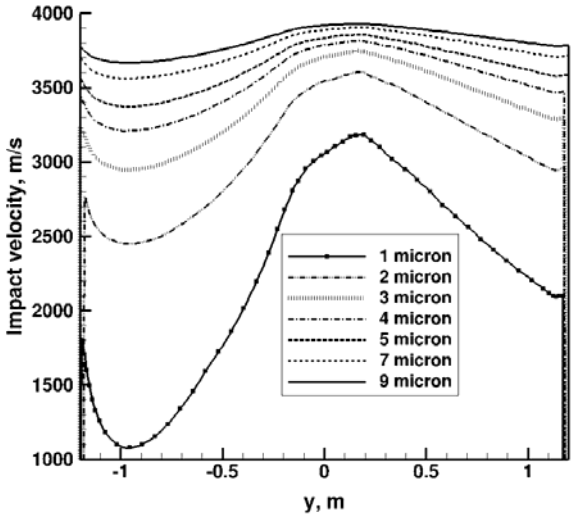

Figure 6. Impact velocity as a function of particle size, 35 km trajectory point

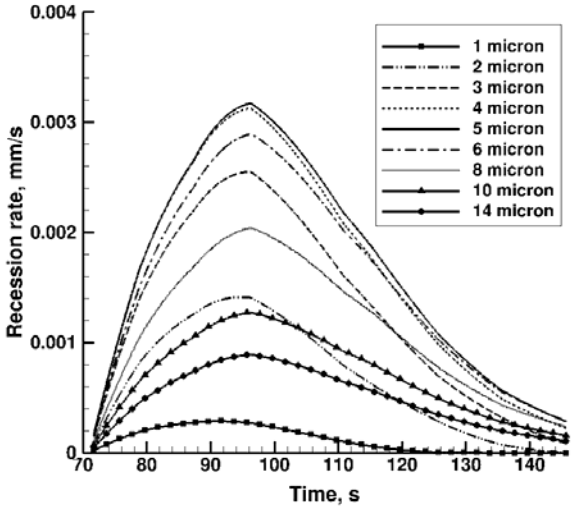

Figure 7. Dust surface recession rates as a function of particle diameter.

The Schiaparelli heatshield consisted of Norcoat Liège insulating tiles, an ablative material composed of resin and cork, but properties for this TPS material are not currently available in the Icarus material database. For the Schiaparelli dust erosion analysis, Phenolic Impregnated Carbon Ablator (PICA) [17] was used to approximate the heatshield material. The switch to PICA affects the amount of surface recession due to charring ablation predicted by Icarus but has no effect on the amount of dust particle erosion because the damage models presented in Section 5 are derived for a single material.

Using inputs provided by the particle trajectory code, the Icarus code computed the material response of the Schiaparelli capsule along its entry trajectory from 50 to 18 km altitude. The equation for AVCOAT shown in Eq. (8) was used to compute impact damage. The largest dust surface erosion occurs at the stagnation point. The recession rate at the stagnation point due to dust particle impacts for various dust particle diameters is shown in Fig. 7. The greatest rate of surface recession is caused by the 4- and 5-micron diameter particles, but all of the particle diameters with the exception of 1-micron particles show recession rates greater than 25% of the peak value meaning that all of them are contributors to the overall surface recession. There are fewer of the larger diameter particles, but each one does significantly more damage than do the smaller particles. The maximum rate of dust erosion recession occurs at the 35 km trajectory point.

Along with the surface recession due to dust particle impacts, the Icarus code also predicted the recession due to charring ablation of the PICA heatshield between 50 and 18 km altitude. The cumulative recession for both char and dust impact erosion components as a function of time are shown in Fig. 8. The majority of the char recession occurs at altitudes above 30 km. The value of char recession asymptotes out after this point to a value of about 2.6 mm. Due to the conflicting trends of increasing mass mixing ratio and decreasing freestream velocity, there is still significant dust erosion at altitudes of 23-25 km. The total dust erosion at the stagnation point was about 1 mm, or 40% of the char recession value.

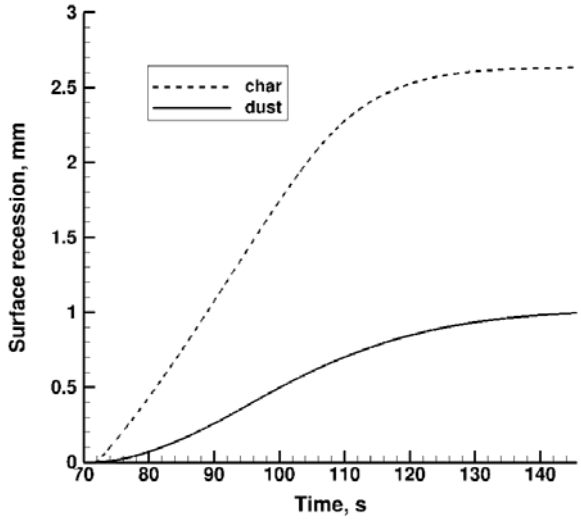

Figure 8. Total surface recession due to charring ablation and dust particle impacts.

9. CONCLUDING REMARKS AND FUTURE WORK

This paper provided an overview of the equations and modeling assumptions that go into an analysis of the heatshield erosion due to dust particle impacts for a spacecraft entering the Martian atmosphere. These models and assumptions were applied to computing the surface erosion due to dust particle impacts on the heatshield of the ExoMars Schiaparelli capsule during a representative dust storm in the Martian atmosphere. The erosion due to dust particle impacts at the stagnation point was estimated to be about 1 mm, which was about 40% the value of recession due to charring ablation. Future work will include applying the Lagrangian particle tracking capability in the DG code from Ref. [13] to the Schiaparelli entry to compare results between one-way and two-way particle-fluid coupling. It is also necessary to examine sensitivity of results to underlying model assumptions, like the spherical particle drag and heating correlations. When the DLR GBK experimental data becomes available, new dust erosion damage correlations will be developed based on appropriate thermal protection material data and incorporated into the Icarus material response code.

10. REFERENCES

[1] Zurak R. W., "Martian Great Dust Storms: An Update", *Icarus., 32,* 288-310, 1982.

[2] Toon, O.B., Pollack, J.B., and Sagan, C., "Physical Properties of the Particles Composing the Martian Dust Storm of 1971-1972," *Icarus*, Vol. 30, pp. 663-696, 1977.

[3] Papadopoulos, P., Tauber, M.E., and Chang, I-D., "Heatshield Erosion in a Dusty Martian Atmosphere," *Journal of Spacecraft and Rockets*, Vol. 30, pp 140-151, 1993.

[4] Palmer, G., Chen, Y-K., Papadopoulos, P., and Tauber, M., "Reassessment of Effect of Dust Erosion on Heatshield of Mars Entry Vehicle," *Journal of Spacecraft and Rockets*, Vol. 37, pp. 747-752, 2000.

[5] Heavens, N., Richardson, M., Kleinbohl, A., Kass, D., McCleese, D., Abdou, W., Benson, J., Schofield, J., Shirley, J., and Wolkenberg, P., "The vertical distribution of dust in the Martian atmosphere during northern spring and summer: Observations by the Mars Climate Sounder and analysis of zonal average vertical dust profiles," *Journal of Geophysical Research*, Vol. 116, pp. 1-23, 2011.

[6] Kahre, M.A., Hollingsworth, J.L., Haberle, R.M., and Murphy, J.R., "Investigations of the variability of dust particle sizes in the martian atmosphere using the NASA Ames General Circulation Model," *Icarus*, Vol. 195, pp. 576-597, 2008.

[7] Conrath, B.J., "Thermal structure of the Martian atmosphere during the dissipation of the dust storm of 1971," *Icarus*, Vol. 24, pp. 36-46, 1975

[8] Forget, F., Hourdin, F., Fournier, R., Hourdin, C., Talagrand, O., Collins, M., Lewis, S.R., Read, P.L., and Huot, J.-P., "Improved general circulation models of the Martian atmosphere from the surface to above 80 km," *Journal of Geophysical Research*, Vol. 104, pp. 155-175, 1999.

[9] Flaherty, R.E., "Impact Characteristics in Fused Silica", AIAA Paper 69-0367, April 1969.

[10] Christiansen, E.L. and Ortega, J.,"Hypervelocity Impact Testing of Shuttle Orbiter Thermal Protection System Tiles," AIAA Paper 90-3666, Sept. 1990.

[11] Henderson, C.B., "Drag Coefficients of Spheres in Continuum and Rarefield Flows," *AIAA Journal*, Vol. 14, pp. 707-708, 1976.

[12] Saito, T., Marumoto, M., and Takayama, K., "Numerical Investigations of Shock Waves in Gas-Particle Mixtures," *Shock Waves*, Vol. 13, pp. 299-322, 2003.

[13] Ching, E., Brill, S., Lv, Y., and Ihme, M., "Development of a Lagrangian Particle Tracking Method for High-Order Discontinuous Galerkin Schemes," AIAA Paper 2018-0360, Jan. 2018.

[14] Schulz, J.C., Stern, E.C., Muppidi, S., and Palmer, G.E., "Development of a Three-Dimensional, Unstructured Material Response Design Tool," AIAA Paper 2017-0667, 2017.

[15] Gülhan, A., Thiele, T., Siebe, F., Kronen, R., and Schleutker, T., "Aerothermal Measurements from the ExoMars Schiaparelli Capsule Entry," *Journal of Spacecraft and Rockets*, Vol. 56, pp. 68-81, 2019.

[16] Wright, M. W., White, T., and Mangini, N., "Data Parallel Line Relaxation (DPLR) Code User Manual Acadia – Version 4.01.1," NASA/TM-2009-215388, October 2009.

[17] Tran, H., Johnson, C., Rasky, D., Hui, F., Chen, Y.-K., and Hsu, M., "Phenolic Impregnated Carbon Ablators (PICA) for Discovery Class Missions," AIAA Paper 96-1911, 1996.